Application of schlieren interferometry to temperature measurements during laser welding of high-density polyethylene films

João M. P. Coelho, Manuel A. Abreu

INETI - DOP, Estrada do Paço do Lumiar 22, 1649-038 Lisbon, Portugal

F. Carvalho Rodrigues

NATO Headquarters, Division of Scientific and Environmental Affairs, B-1110, Brussels, Belgium (on leave from Universidade Independente, Faculdade de Ciências de Engenharia, Av. Marechal Gomes da Costa, Lote 9, 1800-255 Lisboa, Portugal)

Schlieren interferometry is found to be an alternative tool for temperature measurement during thermoplastic laser welding with regard to methods based on thermocouples or optical pyrometers. In fact these techniques are not easily applied when materials to be processed have reduced thickness, negligible heat conduction and low emissivity, as is the case of welding high-density polyethylene films with 10.6 μm CO_2 laser radiation, even if the method reaches its applicability limit after about 1 s of the interaction process. The schlieren method provides the means and the results to probe the thermal variations of the laser-thermoplastic interaction on both surface and interface between the sample material and air.

120.0120, 120.3180, 120.6780, 120.6810

1. Introduction

The development of specific methodologies for obtaining temperature distribution on a medium, gaseous, liquid or solid, has long been a goal for different scientific areas.

To know temperature distribution during materials processing by laser radiation is a fundamental step in understanding the physical processes involved, as well as in validating any theoretical model. This is especially important when the laser radiation is that emitted by a CO_2 laser, because physical mechanisms present in its interaction with materials are mainly thermal. Usual methods to measure temperature involve the use of thermocouples or optical pyrometers. These devices are widely used and their application well studied. However, some problems arise when applying them.

Thermocouples need to be applied directly on the sample or as close as possible. This involves some danger of direct interaction between laser radiation and the device whenever the material has poor heat conduction capability. Also, most processing is performed dynamically. Practical difficulties in terms of local instrumentation and contact probing for a moving sample present a severe limitation in most of the cases. Optical pyrometers do not share these problems since they are non-contact sensors. However, whenever the material's emissivity is not high enough they are difficult to apply.

So, the application of these methods to laser processing of materials with reduced thickness, poor heat transmission and low emissivity is, at least, problematic.

This is the case of welding superposed transparent thermoplastics films with 10.6 μm laser radiation, the reason for which the application of an alternative method based in the interference phenomena, was employed.

Interferometric methods have long being used in thermal analysis through visualization of refractive index changes. For example, Mach-Zender and shearing plate interferometry are commonly used to analyze flames[1,2] and heat transfer between objects[3,4]. However, their application to temperature measurement during laser processing of materials has not been widely studied. In order to fulfill this gap, this paper, reports the application of schlieren interferometry method based on the shearing plate interferometer to the welding of thermoplastic films.

2. Theory

Gaussian laser beam propagation in a non-homogeneous medium, with spatially varying index of refraction, can be described by the ray equation taking the form[5]

$$\frac{d}{dS}\left(n_{ref} \frac{d\delta}{dS} \right) = \nabla_{\perp} n(r,t) \tag{1}$$

where δ is the perpendicular displacement of the beam from the initial position, $\nabla_{\perp} n(r,t)$ the refraction index gradient perpendicular to the ray path, S, and n_{ref} the reference index of refraction (value of undisturbed medium).

The refractive index of air depends on both temperature and pressure. When air is heated it becomes optically non-homogeneous, showing local gradients on the index of refraction, and producing perturbations on the radiation wave front, and thus changing the original beam path. The schlieren technique makes these perturbations readily visible and quantifiable. Since the XVII century, when Robert Hook associated it to the scintillation of the stars[6], until the

development of gradient-index lenses (GRIN), several procedures have been used and adapted to analyze and apply schlieren phenomena. One is based on interference and uses a lateral shearing interferometer[7,8,9,10]. The resulting method is known as schlieren interferometry[1,7,8,11,12,13].

In all schlieren technique applications, a lens (or a mirror) is required to produce a polar diagram of deflections around a pole, which is either its focus, or the image of an aperture. In order to visualize and measure the deflections, the points in the polar diagram have to be "marked" making use of a spatial mask. This mask is either periodic (slit grid, prism of quartz) or aperiodic (knife-edge, graded filters, phase plate). In either case, when the sampling needs to be made at smaller phase intervals, the methods are limited by diffraction.

Schlieren interferometry solves this problem by using diffraction properties rather than avoiding them to perform the measurement and by introducing an interferometer in the schlieren focus. The main advantages of using a lateral shearing interferometer are its simplicity and its small size.

2.1 Schlieren interferometry

Let us consider the schematic shown on fig. 1. A plane wave-front laser beam goes through the inspection area, $\mathscr{S}$, being focused on a plate by a lens, $\mathscr{L}$, with focal distance *f*. After being split in two wave fronts at the first surface (at point *F*), the two waves reflected by the faces of the plate (at *F* and *F'*) will interfere. This interference is visualized in the observation plane, $\mathscr{O}$. To find the location of a fringe on this plane it is necessary to calculate the optical path difference, δ, between rays arriving at each point of the plane $\mathscr{O}$. For a point *P* on the observation plane, having two images P_1 and P_2 in the plane of observation, δ is given by

$$\delta = \left[\left(P_2A + AF + n(FF' + F'F'') + F''P\right] - \left(P_1B + BF + FP\right) + \frac{\lambda}{2} \tag{2}$$

where n is the plate refractive index and $\lambda/2$ represents the advance in phase produced by the air/glass reflection at F and λ is the radiation wavelength. Taken in consideration, the interferometer's shear, P_1P_2, and tilt, PP', Carvalho'Rodrigues[11] and Temple[12] demonstrated that

$$\delta = \frac{h^2u^2(i)}{2M\,f} + 2h\left[n^2 - \sin^2(i)\right]^{1/2} + \frac{\lambda}{2} \tag{3}$$

where $u(i)$ is a function of the geometry of incidence, h is its thickness and M the system's linear magnification. The function $u(i)$ is defined as

$$u(i) = \frac{\sin(2i)}{\left[n^2 - \sin^2(i)\right]^{1/2}} \tag{4}$$

so the interferometer's shear, S, is given by

$$S(i) = \frac{h\,u(i)}{M} \tag{5}$$

Shear is defined as the lateral separation between images of a point of the plane of observation at the source side.

Although equation (3) permits the calculation of the fringe position, it is desirable to calculate independently the fringe separation, as it is directly related to the interferometer's sensitivity and spatial resolution. So, differentiating (3) in i, we have

$$\frac{d\delta}{di} = -h\,u(i)\left[1 - \frac{h\,u'(i)}{M\,f}\right] \tag{6}$$

where $u'(i)$ is the derivative of $u(i)$. When $d\delta$ is equal to one wavelength, di is the angular distance between fringes; their spatial distance being $(M\,f)\,di$. Then

$$di = -\frac{\lambda}{h\,u(i)\left[1-\frac{h\,u'(i)}{M\,f}\right]} \tag{7}$$

This equation shows that the distance between fringes varies along the field of view but that variation can be reduced if $h<<Mf$ and choosing an angle i_0 (angle of incidence of a ray passing through the axis of the optical system) for which $u(i)$ is a maximum.

When a non-uniform field of index of refraction is present in the test zone, the path difference at points on the plane of observation is changed and, as a consequence, the fringe pattern is altered. Two types of alteration can be present. When the index of refraction has a strong variation the splitting, washing out of fringes and variations of intensity from fringe to fringe are observed. In these conditions the interferometer no longer behaves as a schlieren interferometer[11,12]. If the gradients of refractive index are small, the interferometer is not essentially altered. The fringe position is altered according to the variation in path difference due to a change of incident angle.

Then, if a light ray passing through a point in the test plane is deflected by di', the incident angle has a deviation of di=di'/M, assuming that the distance between the point and the optical axis is much lower than f and di' is small. Under those conditions, it is possible to obtain the following relation[1,11]

$$di' = \left(\frac{\Delta P}{\Delta(O'P)}\lambda\right)\frac{M}{h}\frac{1}{u(i)\left[1-\frac{(O'P)^2+2(O'P)Mf\,\mathrm{cotan}(i_0)}{2\left[Mf\,\mathrm{cotan}(i_0)+(O'P)\right]^2}\right]} \tag{8}$$

where ΔP is how much a fringe moved with a disturbance di', and $\Delta(O'P)$ is the fringe's separation.

2.2 Refractive index measurements

Under the conditions of a schlieren interferometer, the expression (1) becomes

$$di' = -\int \frac{1}{n}\frac{dn}{dz}dz \tag{9}$$

at the observation plane. Defining the relative (to air) refraction index as $\delta_n = n-1$, and assuming that $\delta_n << 1$ (or $\delta_n + 1 \approx 1$), relation (9) can be simplified to

$$di' = -\int \frac{d\delta_n}{dz}dz \tag{10}$$

Knowing the angular deflections *di'* it is possible to have the refractive index gradients through an Abel inversion[13,14,15]. This transforms data resultant from a projection on a local distribution of one parameter[16,17,18,19,20]. For a spherical symmetry, the Abel function is

$$di'(z) = 2\int_z^{R0} \frac{r\, d\delta_n(r)}{\sqrt{r^2 - z^2}}dr \tag{11}$$

and its inversion

$$d\delta_n(r) = -\frac{1}{\pi}\int_r^{R0} \frac{\frac{\partial di'(R)}{\partial R}}{\sqrt{R^2 - r^2}}dR \tag{12}$$

where R represents a radial coordinate, $r=(R^2+z^2)^{1/2}$, and R_0 the radius where $d\delta_n/dr=0$. The calculation of the refractive index was then carried out by integration of the set of discrete values of

$$\frac{\partial \delta_n}{\partial r} = \left(\frac{\partial \delta_n}{\partial r}\right)_{r_k} \tag{13a}$$

$$\delta_n(r_j) = \delta_n(r_K) + \sum_{k=j}^{K}(r_{k+1} - r_k)\left(\frac{\partial \delta_n}{\partial r}\right)_{r_{k+1}} \tag{13b}$$

2.3 Temperature measurements

Changes in refractive index of a medium can be due to several factors, such as changes of pressure or temperature. The formation of an acoustic wave can influence the resulting deflection in two ways: by creating an adiabatic compression or a pressure gradient. The acoustic wave propagates from the interaction region to the region crossed by the probe beam, raising the temperature by adiabatic compression, and the resulting gradient deflects the beam. This wave can also contribute to the deflection due to the pressure generated on the irradiated surface; then, the pressure wave propagates to the inspected region and the probe beam is deflected due to the refractive index dependence on pressure.

So, the analysis of the conditions related with the heating process, namely the laser beam and irradiated material thermal characteristics, is needed to quantify the influence of the acoustic contribution. The acoustic relaxation time, τ_{ac}, is given by[22]

$$\tau_{ac} = \frac{r}{2^{1/2} c_s} \tag{14}$$

while the thermal relaxation time, τ_t, by

$$\tau_t = \frac{r^2}{4k} \tag{15}$$

where r is the radius of the beam used for sample irradiation, c_s the speed of sound in the inspected medium, and k the thermal diffusivity of the material. Considering the welding of a

thickness high-density polyethylene (HD PE), using a CO_2 laser beam with r=0.8 mm, and c_s=340 m/s, and k=0.16x10^{-6} m^2/s, we have τ_{ac}=2 μs and τ_t=1 s. So, in this case, the change in temperature is slower than the time necessary for the fluid to expand or contract. Then, the influence of the acoustic wave can be neglected. Also, and under the same conditions, the theory presented by Jackson[23] reports that the influence of pressure change on air is about 10^{-11} that of thermal diffusion. This allows us to conclude that, at the conditions for which the method is to be tested, changes on the refractive index can be related only with thermal changes.

Then, from the refractive index distribution obtained from the schlieren interferometry, the air temperature, T_a, can be determined by using a proper relation. In this work the following relation has been used[24]:

$$n(T_a) = 1 + \frac{(n_{ref} - 1)\, p_{atm}}{1 + 3.4785 \times 10^{-3} (T_a - 15)} \tag{16}$$

when the temperature is expected to be <1000 K. This expression is empiric, and considers the temperature in Celsius and the atmospheric pressure, $p_{atm,}$ in atm. The reference refractive index, n_{ref}, for the probe beam wavelength, λ_p, in μm, is

$$n_{ref} = 1 + \left(6432{,}8 + \frac{2949810\lambda_p^2}{146\lambda_p^2 - 1} + \frac{25540\lambda_p^2}{41\lambda_p^2 - 1} \right) \times 10^{-8} \tag{17}$$

For temperatures between 1000 K and 9500 K, the relation considered is[25]:

$$n(T_a) = 1 + (n_{ref} - 1) \left(\frac{p_{atm}}{96095.43} \right) \left[\frac{1 + 10^{-8} (0.601 - 0.00972\, T_a)\, p_{atm}}{1 + 0.003661\, T_a} \right] \tag{18}$$

These relations, (16) and (18), can be applied to situations with constant low humidity[24,25] as the ones found in the experimental set-up area.

Knowing the temperature distribution in the air, the relation[26]

$$T_a(z,t) = T + (T_{amb} - T)\left[\frac{3}{2}\frac{z}{\delta_T(t)} - \frac{1}{2}\left(\frac{z}{\delta_T(t)}\right)^3\right] \tag{19}$$

with $\delta_T(t)=4.52Pr^{-1/3}(\nu_a t)^{1/2}$, allows us to obtain the temperature on the sample's surface: *T*. *Pr* is the Prandtl number and ν_a the fluid's cinematic viscosity.

3. Experimental Setup

Welding experiments were made using 10 μm and 30 μm thickness HD PE transparent samples processed by a 10.6 μm wavelength laser beam with up to 42 W power and 0.8 mm beam radius on the sample. The sample is moved at 0.042 m/s by an X-Y table.

The schlieren interferometer is applied as it is shown in the schematic of fig. 2. A He-Ne laser beam (λ_p=632.8 nm) is filtered, expanded and collimated (resulting in a 8mm diameter cross section), being directed parallel to the processing area. After, a lens (*f*=55 cm) focuses it onto a plate (*n*=1.6, *h*=2.0 mm, i_0=70º), with the resulting reflection pattern projected on a target, 2.35 m away from the interaction area. The distance between the plate and the target is equal to the lens focal length, *f* (so, *M*=1). The initial pattern has 28 fringes/cm separated by 0.35 mm. A CCD camera with 100Hz acquisition rate was used to record the pattern.

To reduce the influence on the method of changes in weld seam thickness, as processing occurs, the probe beam is made to pass at a small distance (about 0.5-1 mm) from the sample's surface.

4. Results

Fig. 3 shows some patterns obtained during the welding procedure of 10 μm thickness samples. It was observed that about 1s after the beginning of the process, fringes start to separate, to disappear and there are intensity changes from fringe to fringe. This, as stated previously, indicates that the interferometer no longer behaves like a schlieren interferometer due to an intense change in refractive indexes. At instant 1.8 s the lower limit of the pattern has a parabolic shape of the type $z=Ay^2+By+C$, with $A<0$ and $B^2-4AC>0$ as can be seen on fig. 4, and until the end of the processing, no further significant changes are observed. This fact, in accordance with Bialkowski[22], illustrates the lens effect that appears after the initial moments, and limits the method applicability to about 1s.

The linear displacement of each fringe was measured from the acquired images and allowed the determination of the angular deviation by application of relation (8). Then Abel-inversion was applied and the relative refractive index determined after proper numerical integration. An example of resulting data for $y=0$ (line passing by the pattern's vertical center) and $t=0.39$ s is presented in fig. 5. Air temperature distribution could then be determined. Fig. 6 shows the result after handling the experimental data in the case of the previous example (fig. 5), as well as respective major and minor errors (propagation of a 0.05mm error on determining the fringe's linear displacement).

Also, the method was applied for the same welding parameters, so average values were obtained. It was observed that standard deviation increases as the limit of applicability of the method approaches ($t\approx1$ s) and for the position nearer to the sample's surface. An example of values obtained for $t=0.39$ s can be seen in fig. 7. Fig. 8 shows the temperature distribution at the air above the thermoplastic for several instants from the beginning of the process until

approaching the method's applicability limit. Applying relation (19) the temperature on the sample's surface is determined, and the result can be seen in fig. 9.

5. Method validation

Based on the refractive index gradient given by expression (12) e through relation (11) it is possible to predict the deflection that a beam crossing above the interaction zone would suffer: to curves $d\delta_n(r)$ found, the Abel function is applied, and a $di'(z)$ distribution (or $di(z)$, as M=1) obtained relative to the test zone. This way it is possible, from schlieren interferometry results, to obtain the deflection values to each point of the considered probe beam cross section. Comparing these predictions to experimental data allows validation of the method. Fig. 10 shows the schematic used to experimentally obtain the total deflection of a laser beam. The probe beam, with 1mm diameter, is emitted by the He-Ne laser and its deflection is projected on a target, being recorded by the CCD camera. In order to avoid interference between the welding seam and the probe beam this is directed about 0.5 mm above the thermoplastic surface. Then, $di(z)$ is determined for three positions: z=0.5 mm, z=1.0 mm and z=1.5 mm, and the results are plotted in fig. 11. Deflection of central point (z=1.0 mm) with time can be described by equation di(mrad)=1.099t(s)+0.016 for 10 μm samples and di(mrad)=1.093t(s)-0.042 for 30 μm samples. Assuming that these relations are valid until t=1.8s (after which the schlieren pattern shows no significant further changes), the calculated deflection is 2.0 ±0.3 mrad and 1.9±0.3 mrad respectively. The observed deflections were 1.7±0.5 mrad and 1.9±0.5 mrad. So, and despite of the associated error, results are coincident.

Based on the data resulting from the application of Abel function it is also possible to predict the deflected beam dimensions and to compare them with those experimentally observed. This comparison is presented in fig. 12, where the shape of the initial (undisturbed) beam cross

section it is also plotted. The agreement between the predicted and experimental values can again be observed.

6. Conclusions

A schlieren interferometry method was applied to the measurement of temperature during laser radiation welding of transparent HD PE samples. This method is based on a lateral shearing interferometer and allows the thermal characterization of the interface between the irradiated thermoplastic surface and the air. This allowed the temperature distribution on the sample's surface during processing to be obtained.

The method was validated through the comparison between the predictions made by the application of Abel function to schlieren interferometry results, and the experimental deflection analysis data.

Results allow the conclusion that schlieren interferometry can be a powerful tool when used in thermoplastics laser radiation welding, permitting a better understanding of related thermal phenomena. However, it was also observed that, when refractive index gradients became too high, the method reaches its applicability limit, no longer behaving as a schlieren interferometer. Also, changes in the weld seam positioning during the weld process can introduce errors in the results.

This method can be easily applied in laboratorial and industrial environments and it represents an alternative to thermocouples and optical pyrometers. Also, deflection diagnostic techniques can be used in conjunction with the schlieren method, it being possible to, alternatively, use this deflection method after proper calibration through schlieren interferometry. This would be advantageous in industrial applications where simpler deflection set-up would be preferred.

Acknowledgements

The authors wish to thank their colleagues Dr. Jerónimo Silva and José Rabaça for their collaboration in this work.

References

1. M. R. Barrault, G. R. Jones, F. Carvalho Rodrigues, "Practical arcing environments arc plasma diagnostics", in *Proceedings of 7th Yugoslav Symposium and Summer School on the Physics of Ionized Gases*, V. Vujnovic, ed. (Rovinj, Yugoslavia, 1974), **1**, pp. 701-807.
2. B. VanDerWege, C. O'Brien, S. Hochgreb, "Quantitative shearography in axisymmetric gas temperature measurements", J. Opt. Lasers Eng., **31**, 21-39 (1999).
3. M. Pavelek, E. Janotkova, "Interferometric research of heat transfer at air jet from ventilating outlets", in *Proceedings of 6th International Symposium Ventilatium 2000*, Sointu Hiltumen, ed. (Helsinki, Finland, 2000), **2**, pp. 179-181, http://dt.fme.vutbr.cz/~pavelek/00fin-m.doc.
4. M. Pavelek, E. Janotkova, "Research of dynamic temperature fields by means of Mach-Zender interferometer", in *Proceedings of International Congress of Chemical and Process Engineering, CHISA'98,* Process Engineering Publisher (Prague, Czech Republic, 1998), **4**, paper P1.146, http://dt.fme.vutbr.cz/~pavelek/98CHISAm.doc.
5. Reeta Vyas, R. Gupta, "Photothermal lensing spectroscopy in a flowing medium: theory", Appl. Opt., **27**, 4701-4711 (1988).
6. J. Rienitz, "Schlieren experiment 300 years ago", in *Selected Papers on Schlieren Optics*, Jurgen R. Mayer-Arendt, ed, SPIE MS **61**, 10-12 (1992).
7. J. Araújo Silva, A. Fernandes Arriegas, *Controlo de qualidade em óptica ocular* (M. F. R. Lda., Lisboa, 1992).
8. Daniel Malacara, *Optical shop testing*, (John Wiley & Sons Inc., 1992).

9. H. Schreiber, J. Schwider, "Lateral shearing interferometer based on two Ronchi phase gratings in series", Appl. Opt. **36**, 5321-5324 (1997).
10. S. Siano, R. Pini, R. Salimbeni, M. Vannini, "A diagnostic set-up for time-resolved imaging of laser-induced ablation", J. Opt. Lasers Eng. **25**, 1-12 (1996).
11. F. Carvalho Rodrigues, *Optical diagnostics – high current arcs,* Ph.D. Dissertation (University of Liverpool, Liverpool, 1974).
12. Edward B. Temple, "Quantitative Measurement of Gas Density by Means of Light Interference in a Schlieren System" Journal of the Optical Society of America **47** (1), 91-100 (1957).
13. Gary S. Settles, *Schlieren and Shadowgraph Techniques: Visualizing Phenomena in Transparent Media* (Springer-Verlag, 2001).
14. R. Bracewell, *The Fourier Transform and Its Applications*, 3rd ed. (Mc-Graw-Hill, New York, 1999).
15. Ajay K. Agrawal, Burt W. Albers, and DeVon W. Griffin, "Abel inversion of deflectometric measurements in dynamic flows", Appl. Opt. **38**, 13394-3398 (1999).
16. Manuel Ribau Teixeira, *Processos atómicos em descargas luminescentes de cátodo oco*, Ph.D. Dissertation (Universidade de Lisboa, Lisbon , 1983).
17. Manuel Heitor, Paulo Ferrão, Armando Caldeira-Pires, Duarte Correia, Pedro Maia, "On the development and implementation of a 3D tomographic sensor on an unconfined laboratory combustion system", BRITE/EURAM Project BE95/1708 – Clean Glass IST Technical Report (1999), http://in3.dem.ist.utl.pt/publications/PAPERS/ifrf_report.pdf.

18. K. Green, M. C. Borrás, P. P. Woskov, G. I. Flores III, K. Hadidi, P. Thomas, "Electronic excitation temperatures profiles in an air microwave torch", Plasma Science and Fusion Center, MIT (2001), http://www.psfc.mit.edu/library/01JA/01JA005/01JA005_full.pdf.
19. Philippe Ben-Abdallah, Mohamed Sakami, Vital Le Dez, Jean Bernard Saulnier, André Charette, "Optical remote sensing inside an inhomogeneous axisymetric medium: the absorption field measurement", Appl. Opt., **39**, 411-417 (2000).
20. L. Ciotti, "Inversion of the Abel equation for toroidal density distributions", Astrophysical Letters and Communications, **40**, 85 (2000).
21. Laboratory for Laser Energetics, LLE review, **66**, 66-72 (1996), http://www.lle.rochester.edu/pub/review/v66/v66-abel.pdf.
22. Stephen E. Bialkowski, *Photothermal Spectroscopy Methods for Chemical Analysis*, (John Wiley & Sons Inc., 1996), Chapter 1.
23. W. B. Jackson, N. M. Amer, A. C. Boccara, and D. Fournier, "Photothermal deflection spectroscopy and detection", Appl. Opt., **20**, 1333-1344 (1981).
24. *Zemax – Optical design program user's guide*, (Focus Software Inc., Tucson, 2001). (Cross reference to: F. Kohlraush, Praktishe Physik, **1**, 408, 1968)
25. J. E. Decker, J. R. Pekelsky, "Gauge Block Calibration by Optical Interferometry at the National Research Council of Canada", NRC Internal Report Nº 40002, 6-7 (1997).
26. Bruno A. Boley, Jerome H. Weiner, *Theory of Thermal Stresses* (John Wiley & Sons, 1960).

FIGURE CAPTIONS

Fig. 1. Schematic of lateral shearing interferometry.

Fig. 2. Schematic of the experimental set-up.

Fig. 3. Example of pattern images registered by the CCD camera at different moments in time (processing started at t=0 s) during 10 μm thickness samples' welding.

Fig. 4. Observed parabolic shape of pattern's lower limit after the method applicability limit being reached.

Fig. 5. Example of data sequence as the method is applied: (a) observed angular deflection, (b) refractive index gradients obtained by Abel-inversion, and (c) refractive index map resulting from integration of former data.

Fig. 6. Air Temperature distribution measured by the method above the sample at instant t=0,39 s. Broken lines represent related major and minor errors. (Example of 10 μm thickness samples' welding).

Fig. 7. Average air temperature distribution measured above the sample at instant t=0.39 s for both thicknesses considered.

Fig. 8. Average air temperature distribution measured above the sample at several instants. Example of 10 μm thickness samples' welding.

Fig. 9. Time evolution of thermoplastic's temperature measured at its surface for (a) 10 μm and (b) 30 μm thicknesses samples' welding.

Fig. 10. Schematic of the experimental set-up used for deflection measurements.

Fig. 11. Predicted deflection for probe beam at z=0.5 mm, 1.0 mm and 1.5 mm for (a) 10 μm and (b) 30 μm thicknesses samples' welding. It is also shown the "best fit" equation for central point deflection.

Fig. 12. Probe beam cross-sections: observed before the inspected zone, observed through deflection experiments and predicted from schlieren interferometry results. Example for 10 μm thickness samples' welding.

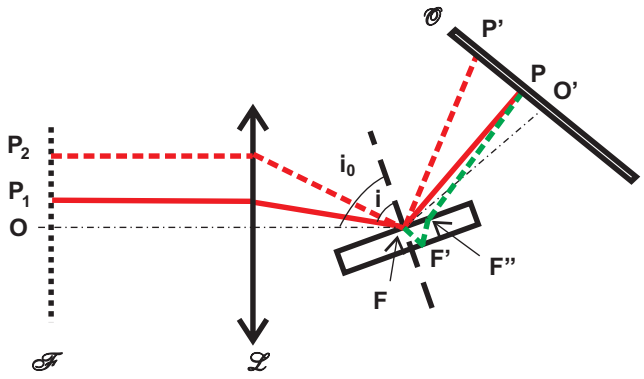

Fig. 1.

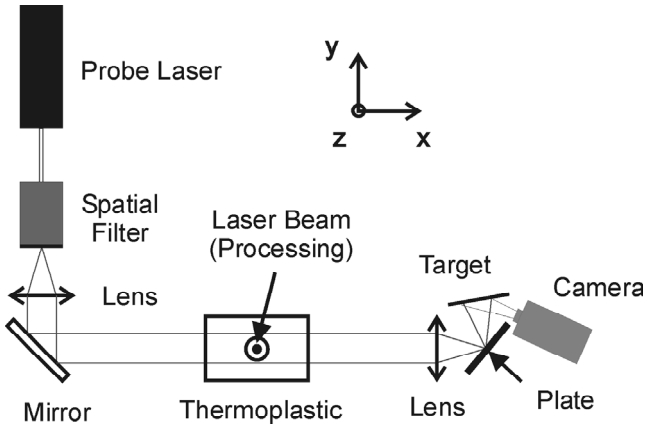
Probe Laser
y
z
x
Spatial
Filter
Laser Beam
(Processing)
Target
Camera
Lens
Mirror
Thermoplastic
Lens
Plate

Fig. 2.

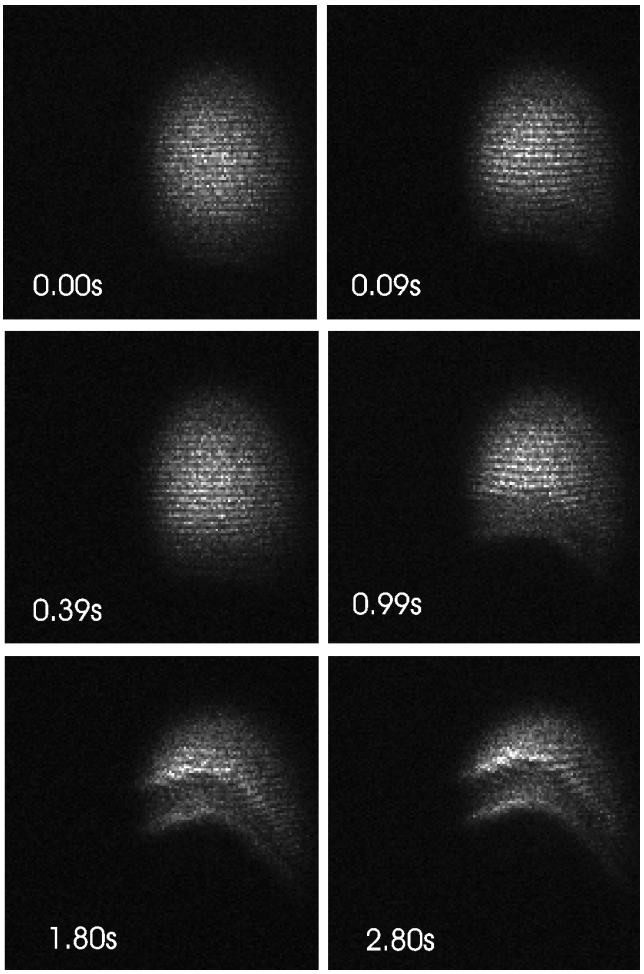

Fig. 3.

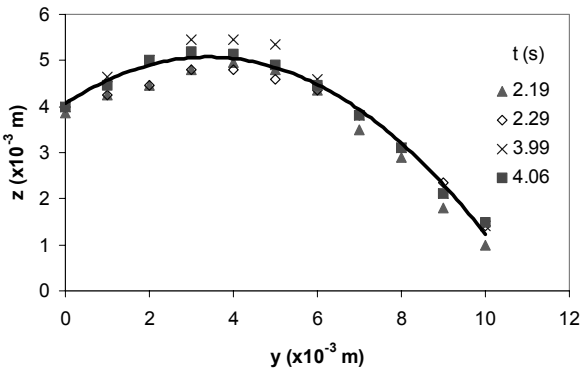

Fig. 4.

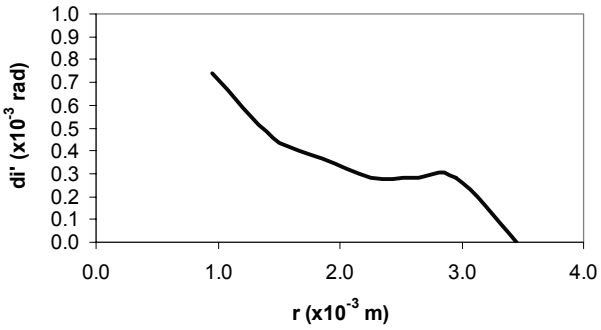

Fig. 5. (a)

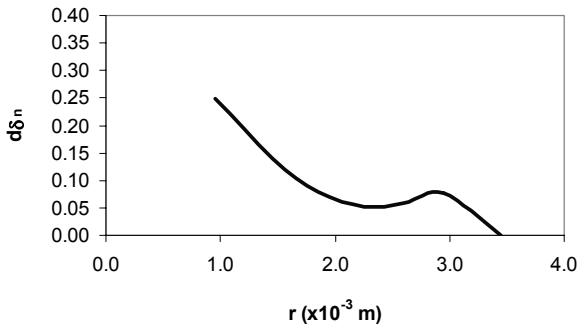

Fig. 5. (b)

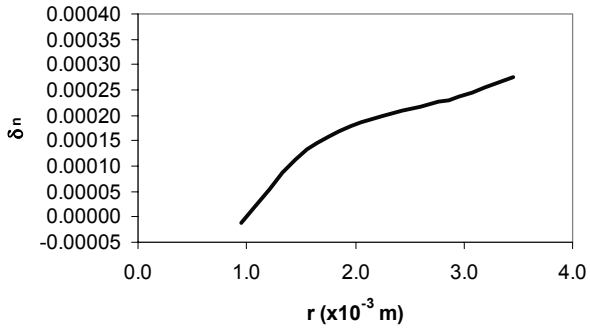
0.00040
0.00035
0.00030
0.00025
0.00020
0.00015
0.00010
0.00005
0.00000
-0.00005
δn
0.0
1.0
2.0
3.0
4.0
r (x10-3 m)

Fig. 5. (c)

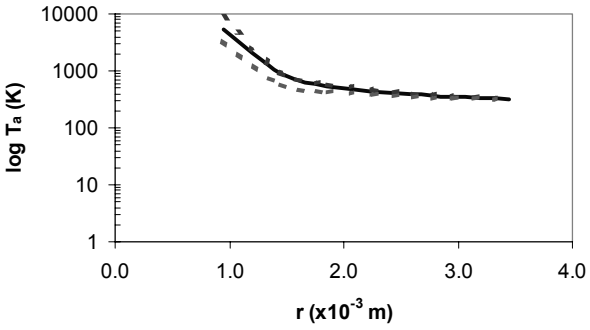

Fig. 6.

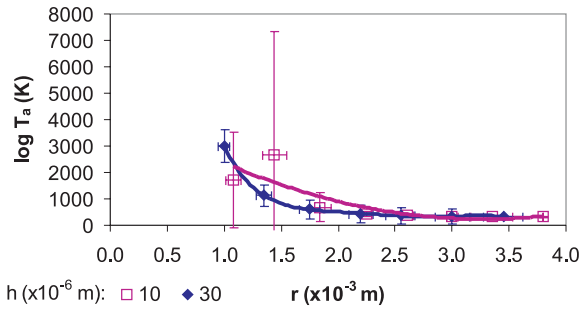
8000
7000
6000
5000
4000
3000
2000
1000
0
log Ta (K)
0.0
0.5
1.0
1.5
2.0
2.5
3.0
3.5
4.0
h (x10-6 m): 10 30
r (x10-3 m)

Fig. 7.

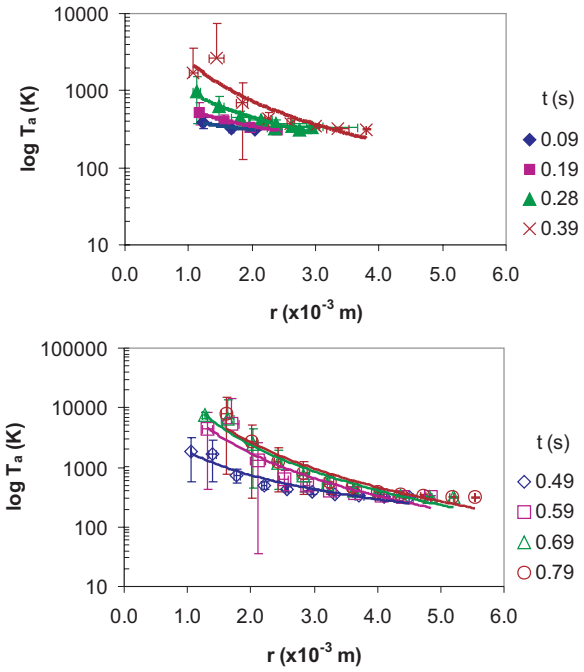
10000
1000
100
10
log Ta (K)
0.0
1.0
2.0
3.0
4.0
5.0
6.0
r (x10-3 m)
t (s)
0.09
0.19
0.28
0.39
100000
10000
1000
100
10
log Ta (K)
0.0
1.0
2.0
3.0
4.0
5.0
6.0
r (x10-3 m)
t (s)
0.49
0.59
0.69
0.79

Fig. 8.

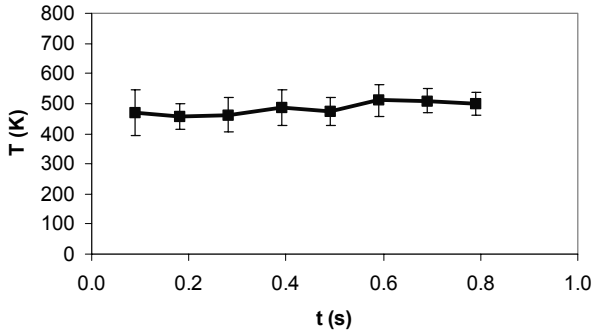

Fig. 9. (a)

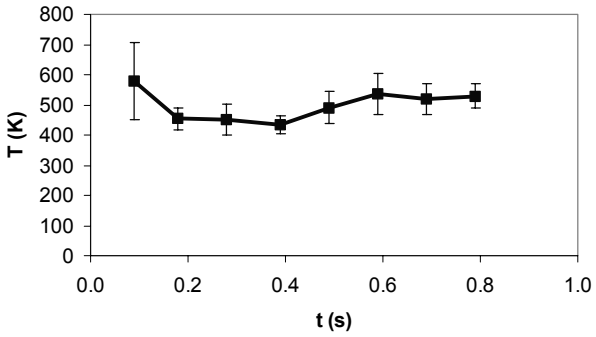

Fig. 9. (b)

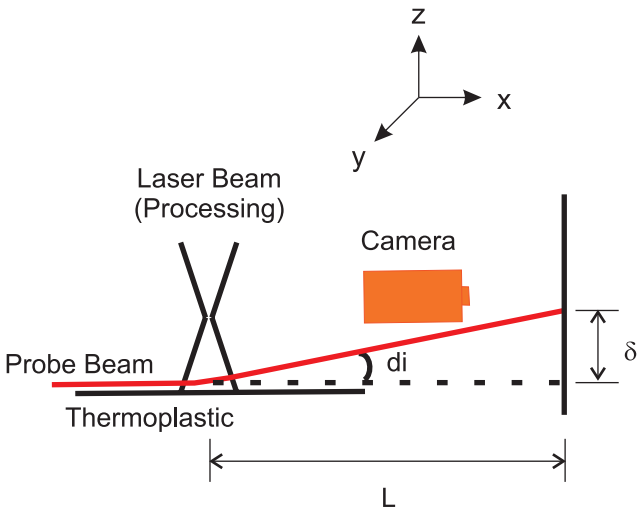
z
x
y
Laser Beam
(Processing)
Camera
Probe Beam
di
δ
Thermoplastic
L

Fig. 10.

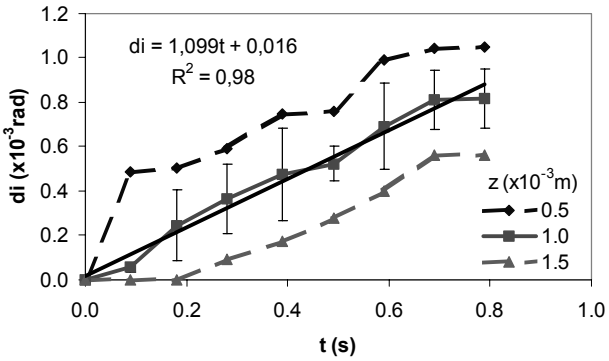
di = 1,099t + 0,016
R2 = 0,98
di (x10-3rad)
t (s)
z (x10-3m)
0.5
1.0
1.5
0.0
0.2
0.4
0.6
0.8
1.0
1.2

Fig. 11. (a)

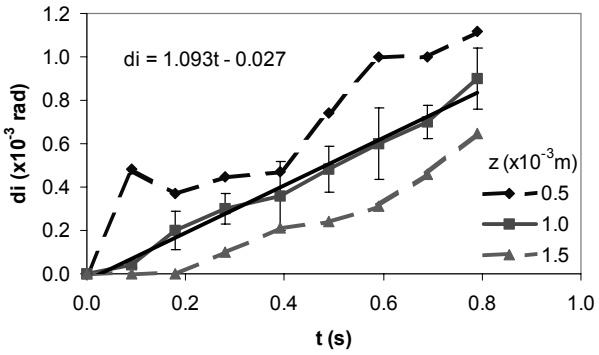

Fig. 11. (b)

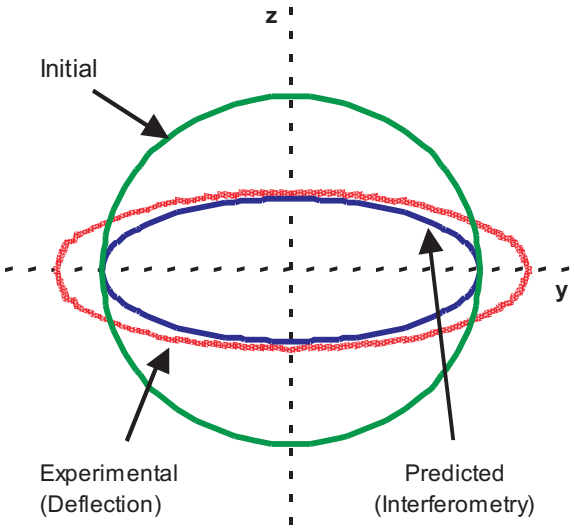
z
Initial
y
Experimental
(Deflection)
Predicted
(Interferometry)

Fig. 12.